Hindawi Publishing Corporation
International Journal of Photoenergy
Volume 2016, Article ID 8172518, 8 pages
http://dx.doi.org/10.1155/2016/8172518

Research Article

Wide-Range Enhancement of Spectral Response by Highly Conductive and Transparent μc-SiO$_x$:H Doped Layers in μc-Si:H and a-Si:H/μc-Si:H Thin-Film Solar Cells

Pei-Ling Chen, Po-Wei Chen, Min-Wen Hsiao, Cheng-Hang Hsu, and Chuang-Chuang Tsai

Department of Photonics, National Chiao Tung University, 1001 University Road, Hsinchu 30010, Taiwan

Correspondence should be addressed to Pei-Ling Chen; daphnechen0822orama@gmail.com

Received 15 April 2016; Accepted 12 July 2016

Academic Editor: Vishal Mehta

The enhancement of optical absorption of silicon thin-film solar cells by the p- and n-type μc-SiO$_x$:H as doped and functional layers was presented. The effects of deposition conditions and oxygen content on optical, electrical, and structural properties of μc-SiO$_x$:H films were also discussed. Regarding the doped μc-SiO$_x$:H films, the wide optical band gap (E_{04}) of 2.33 eV while maintaining a high conductivity of 0.2 S/cm could be obtained with oxygen incorporation of 20 at.%. Compared to the conventional μc-Si:H(p) as window layer in μc-Si:H single-junction solar cells, the application of μc-SiO$_x$:H(p) increased the V_{OC} and led to a significant enhancement in the short-wavelength spectral response. Meanwhile, the employment of μc-SiO$_x$:H(n) instead of conventional ITO as back reflecting layer (BRL) enhanced the external quantum efficiency (EQE) of μc-Si:H single-junction cell in the long-wavelength region, leading to a relative efficiency gain of 10%. Compared to the reference cell, the optimized a-Si:H/μc-Si:H tandem cell by applying p- and n-type μc-SiO$_x$:H films achieved a V_{OC} of 1.37 V, J_{SC} of 10.55 mA/cm^2, FF of 73.67%, and efficiency of 10.51%, which was a relative enhancement of 16%.

1. Introduction

Over the past decade, silicon-based thin-film solar cell technology has become a viable approach for mass production due to its characteristics such as large-scale production, low temperature process, and abundant storage of silicon in the earth crust [1, 2]. However, compared with the mainstream of photovoltaics, the conversion efficiency of silicon-based thin-film solar cells still needs to be improved. One of the approaches is to fabricate multijunction solar cells comprising subcells with absorbers having different band gaps to convert broad-band solar energy into electricity. Among various silicon-based materials, the hydrogenated microcrystalline silicon (μc-Si:H) has been reported as a promising candidate for the absorber of middle or bottom cells in multijunction cells. The μc-Si:H has the advantages of higher optical absorption coefficients at the infrared region and less light-induced degradation than the hydrogenated amorphous silicon (a-Si:H) [3]. Intensive researches have focused on the development of a-Si:H/μc-Si:H tandem solar cells [4–6]. The band gap combination of a-Si:H (~1.8 eV) and μc-Si:H (~1.1 eV) provides a great benefit of utilizing broad sunlight spectrum [6]. However, the absorber thickness of μc-Si:H is relatively thick (~1–3 μm) compared with a-Si:H owing to its nature of indirect band gap. To further improve the efficiency of μc-Si:H solar cells without increasing the thickness of the absorbers, the light management of the solar cells is a critical factor.

Studies have reported that the p- and n-type μc-Si:H are commonly used as doped layers in μc-Si:H solar cells due to its properties of low activation energy and high conductivity, which increased the build-in field and reduced the series resistance of solar cells [7, 8]. However, the optical band gap (E_{04}, the photon energy at which the absorption coefficient is 10^4 cm^{-1}) could only be adjusted in a small range of 1.9~2.1 eV for the doped μc-Si:H layers [9, 10]. Besides, the parasitic absorption of the doped μc-Si:H layers contributes to the loss in photocurrent. To further improve the optical properties of the doped layers, hydrogenated microcrystalline silicon oxide (μc-SiO$_x$:H) has been developed for thin-film solar cells. The

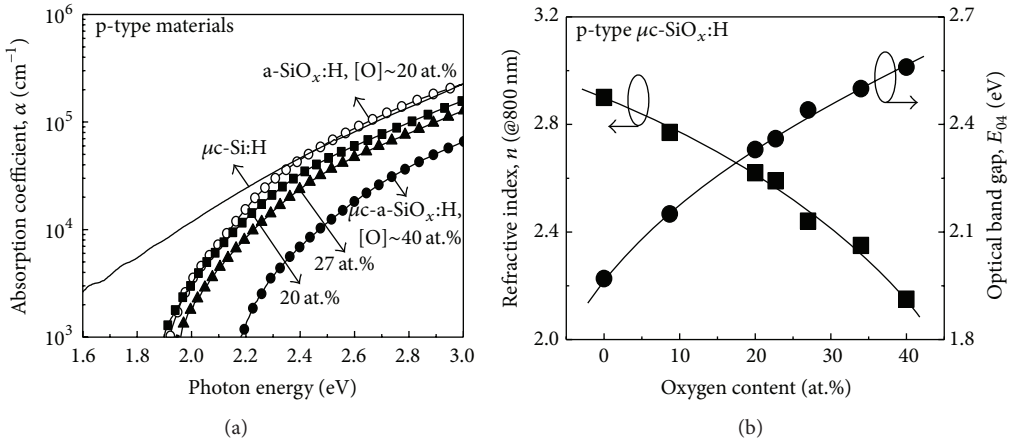

FIGURE 1: (a) Absorption coefficient of a-SiO$_x$:H, μc-Si:H, and μc-SiO$_x$:H with varied oxygen content [O] and (b) the refractive index (n) and the optical band gap (E_{04}) of μc-SiO$_x$:H with varied oxygen content [O].

μc-SiO$_x$:H has been proposed to be a mixed-phase material comprising a-SiO$_x$:H phase and μc-Si:H phase [11, 12]. The oxygen-rich amorphous phase supplied low refractive index and high E_{04}, while the conductive doped μc-Si:H phase provided the low-resistance pathway for carrier transport [12]. The incorporation of oxygen in the silicon network effectively widened the E_{04} and reduced the refractive index. As a result, the doped μc-SiO$_x$:H can be used as doped layers as well as intermediate reflecting layer (IRL), tunneling recombination junction (TRJ) layer, and back reflecting layer (BRL), owing to its tunable optical and electrical properties [13–17].

Nevertheless, excessive oxygen content in μc-SiO$_x$:H film significantly suppressed the crystallization, which adversely affected the electrical property. Reports have shown that compared to μc-Si:H having conductivity of 10~10^2 S/cm and E_{04} of 1.9~2.1 eV, the conductivity of the doped μc-SiO$_x$:H films degraded to 10^{-3}~10^{-4} S/cm as the E_{04} was as high as 2.3 eV [18, 19]. Therefore, to further improve the electrical and optical property by optimizing the deposition conditions were needed for enabling the extensive applicability of the μc-SiO$_x$:H films.

This work aims to efficiently enhance the light absorption in solar cells. The optoelectrical properties of the doped μc-SiO$_x$:H materials as the window and the back reflector layers employed in μc-Si:H single-junction and a-Si:H/μc-Si:H tandem solar cells were investigated.

2. Experimental Details

Silicon-based thin-films were prepared with a single chamber process in multichamber plasma-enhanced vapor deposition (PECVD) system equipped with 27.12 MHz RF power and NF_3 in situ plasma cleaning. Gas mixture of SiH_4, CO_2, B_2H_6, PH_3, and H_2 was used as source gases. The μc-SiO$_x$:H(p) and μc-SiO$_x$:H(n) films were deposited onto Corning EAGLE XG glass substrate at approximately 190°C. The incorporation of oxygen was achieved by introducing CO_2 in highly H_2-diluted SiH_4. The oxygen content, [O], of μc-SiO$_x$:H films was examined by an X-ray photoelectron spectroscopy (XPS). The crystalline volume fraction (X_C) of μc-SiO$_x$:H was calculated from the ratio of the integrated intensities of deconvoluted peaks centered at 480, 510, and 520 cm^{-1} from a Raman spectrum with a probe laser of 488 nm excitation. The optical band gap (E_{04}) was obtained by an ultraviolet-visible-near-infrared spectrophotometer. The refractive indices were estimated from an ellipsometry measurement by applying Fresnel equation. The dark conductivity (σ_d) was measured with coplanar Ag electrodes at room temperature.

The μc-Si:H solar cells were deposited in a superstrate configuration on textured SnO_2:F glass substrate. The structure of μc-Si:H single-junction solar cells was glass/SnO_2:F/μc-SiO$_x$:H(p)/μc-Si:H(i)/μc-SiO$_x$:H(n)/Ag with 1.4 μm thick μc-Si:H absorber. The thicknesses of the absorbers of a-Si:H and μc-Si:H component cells were 240 nm and 1.4 μm, respectively. The Ag electrode was prepared by thermal evaporator with the area of 0.25 cm^2 defined by the shadow mask. The cells were characterized by an AM1.5G illuminated J-V measurement system and an external quantum efficiency (EQE) instrument.

3. Results and Discussion

3.1. Electrical and Optical Properties of Doped μc-SiO$_x$:H Thin-Films. The absorption coefficients of the p-type μc-SiO$_x$:H as a function of [O] are shown in Figure 1(a). Compared to the a-SiO$_x$:H(p), the μc-SiO$_x$:H(p) exhibited lower absorption coefficient owing to the indirect band gap of μc-Si:H phase while the oxygen content was 20 at.% in both cases. In addition, the optical absorption coefficient of μc-SiO$_x$:H(p) shifted toward higher photon energy as the oxygen content was increased from 0 (μc-Si:H(p)) to 40 at.%, which was attributed to the increased a-SiO$_x$:H phase in the films [11]. The n-type μc-SiO$_x$:H layers showed similar trends [20].

The refractive index (n, at the wavelength of 800 nm) and the E_{04} versus the oxygen content are demonstrated in Figure 1(b). As the [O] was increased from 0 (μc-Si:H(p)) to 40 at.%, the E_{04} was increased from 1.97 to 2.56 eV. This can be

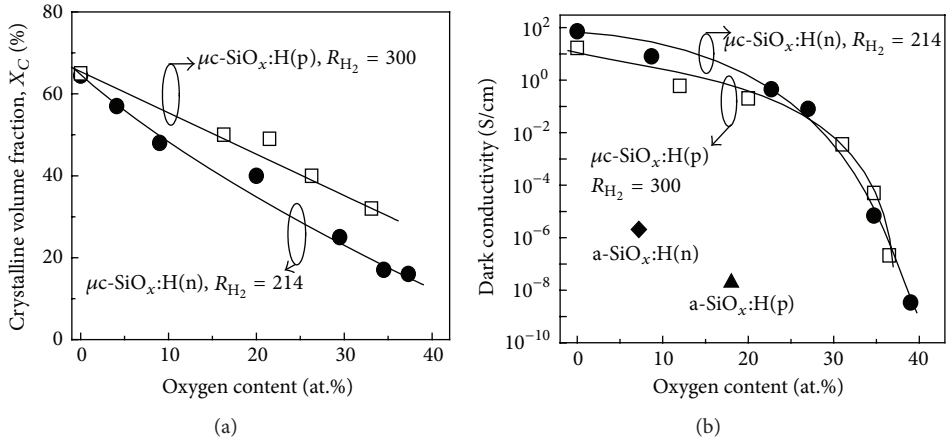

FIGURE 2: (a) Crystalline volume fraction (X_C) of μc-SiO$_x$:H(p) and μc-SiO$_x$:H(n) films versus the oxygen content [O]. (b) Dependence of the dark conductivity (σ_d) on the oxygen content [O] for μc-SiO$_x$:H(p) and μc-SiO$_x$:H(n) films.

ascribed to the increased Si-O bond in a-SiO$_x$:H phase since the bonding energy of Si-O bond was higher than that of Si-Si and Si-H bonds in a-SiO$_x$:H phase. On the other hand, the refractive index was decreased from 2.90 to 2.15 accordingly. The tunable refractive index was beneficial when employing μc-SiO$_x$:H doped layers as the index-matching layer, IRL, and BRL.

The electrical properties of μc-SiO$_x$:H doped layers mainly depended on X_C and doping, which was significantly affected by the deposition conditions in the PECVD system. The dependence of X_C of μc-SiO$_x$:H(p) and μc-SiO$_x$:H(n) films on [O] is shown in Figure 2(a). In the case of μc-SiO$_x$:H(p) with H_2-to-SiH_4 flow ratio (R_{H_2}) of 300, X_C was decreased from 65 to 32% when the [O] was increased from 0 to 33 at.%. Similarly, in the case of μc-SiO$_x$:H(n) with R_{H_2} of 214, as the [O] was increased from 0 to 37 at.%, X_C was decreased from 64% to 16%. This suggested that the incorporation of oxygen into μc-Si:H network suppressed the formation of crystalline phase due to the oxygen-induced defects [21]. It should be noted that R_{H_2} of μc-SiO$_x$:H(p) under similar X_C was higher than that of μc-SiO$_x$:H(n), which can be ascribed to the boron that had more impact on disrupting the crystalline structure than that of phosphorus [22]. It has been reported that the energy-favorable configuration of phosphorus atoms in the Si matrix was tetrahedral, which made phosphorus act as the crystallization centers [23]. In contrast, the boron may adopt other energy-favorable configurations that were not tetrahedral. The inactive boron atoms could segregate to the grain boundaries, which hindered the crystalline formation [24]. Therefore, R_{H_2} of μc-SiO$_x$:H(p) was higher than that of μc-SiO$_x$:H(n) in order to assist the crystallization in our case.

The dependence of σ_d on the [O] for μc-SiO$_x$:H(p) and μc-SiO$_x$:H(n) films was shown in Figure 2(b). In the case of μc-SiO$_x$:H(p), the decreasing trend on σ_d from 16.7 to 2.1×10^{-7} S/cm with the increase [O] from 0 to 36 at.% was observed. In comparison, in the case of μc-SiO$_x$:H(n), σ_d was decreased from 72.4 to 3.4×10^{-9} S/cm as [O] was increased from 0 to 39 at.%. The reduced σ_d can be attributed to the decreased X_C arising from the increased defect density by the oxygen incorporation into the films. Moreover, the doping efficiency was reduced with the decrease in X_C [25], which further degraded σ_d at high [O]. In Figure 2(b), the p-type and n-type a-SiO$_x$:H were also shown for comparison. Regarding p-type layers, it can be seen that σ_d of μc-SiO$_x$:H with [O] of 20 at.% was higher than that of a-SiO$_x$:H with [O] of 18 at.%. Similarly, μc-SiO$_x$:H(n) with [O] of 8 at.% exhibited higher σ_d than a-SiO$_x$:H(n) with [O] of 7 at.%. The significantly enhanced σ_d was due to the crystalline structure of μc-SiO$_x$:H layer which facilitated the carrier transport and the higher doping efficiency in μc-Si:H phase of μc-SiO$_x$:H films compared with the a-SiO$_x$:H doped layers. As a result, μc-SiO$_x$:H(p) with [O] of 20 at.%, E_{04} of 2.33 eV, and the high σ_d of 0.2 S/cm were obtained. Regarding the μc-SiO$_x$:H(n), high σ_d of 0.08 S/cm was obtained as [O] was 27 at.% with lower refractive index of 2.55 (n at 800 nm). μc-SiO$_x$:H(p) and μc-SiO$_x$:H(n) with tunable optical and electrical properties were applied as window layer and BRL in silicon thin-film solar cells, respectively.

3.2. Application of μc-SiO$_x$:H(p) as Window Layer in μc-Si:H Solar Cells. The μc-SiO$_x$:H(p) with varied [O] were utilized in μc-Si:H single-junction solar cells. The EQE and cell reflection are illustrated in Figure 3. With the [O] increased from 0 (μc-Si:H(p)) to 31 at.%, the short-wavelength spectral response was enhanced significantly. This was due to the reduced parasitic absorption loss by using wide-band gap μc-SiO$_x$:H(p) and the increased light-incoupling owing to graded refractive index [26]. The decreased cell reflection in the short-wavelength range with the increasing oxygen content corresponded to the increased EQE in the short-wavelength range. This indicated that the refractive index of μc-SiO$_x$:H(p) (n = 2.7 at 800 nm) in between the front TCO ($n \sim 2$) and the μc-Si:H absorber ($n \sim 3.6$) may act as an antireflection layer by the graded refractive index. The corresponding cell performance of μc-Si:H single-junction solar cells is summarized in Table 1. With the [O] increase from 0 to 31 at.%, the short-circuit current density (J_{SC}) was

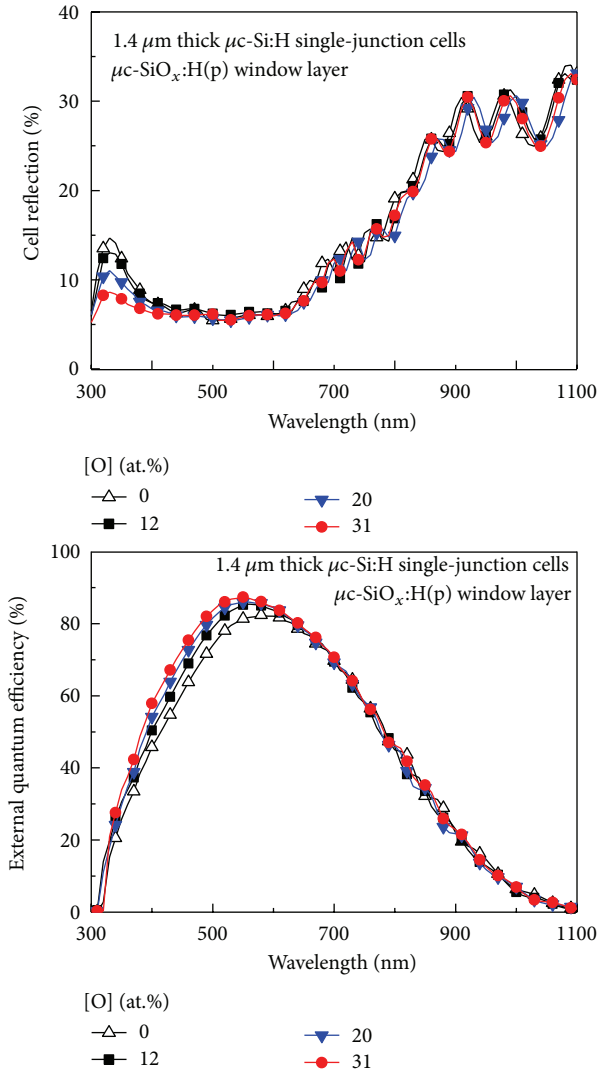

Figure 3: External quantum efficiency of μc-Si:H single-junction solar cells employed μc-SiO$_x$:H(p) with varied oxygen content [O] as window layer and cell reflectance as a function of oxygen content.

increased from 19.73 to 21.62 mA/cm^2. Compared with the cell using μc-Si:H(p) ([O] = 0%), the cell employing μc-SiO$_x$:H(p) with [O] of 12 at.% and 20 at.% exhibited enhancement in fill factor (FF). This can be attributed to the shunt quenching effect by μc-SiO$_x$:H(p) layer which suppressed the carrier recombination at the p/i interface [12, 27]. With [O] increased from 0 to 20 at.%, the open-circuit voltage (V_{OC}) was increased from 0.49 to 0.51 V, which were due to the increase in band gap of μc-SiO$_x$:H(p) window layer. In addition, the utilization of wide-band gap p-layer presented a potential barrier on the conduction band, which suppressed the diffusion of electron across the p/i interface and reduced the carrier recombination in bulk region or at p/i interface, leading to an improved V_{OC} [18]. Further increase in the [O] to 31 at.% resulted in the decrease in V_{OC} and FF, which can be attributed to the increase in oxygen-induced defect states existing near the p/i interface and the decrease in σ_d of

Table 1: Performance of μc-Si:H single-junction solar cells employed μc-SiO$_x$:H(p) with varied oxygen content [O] as window layer.

[O] (at.%)	V_{OC} (V)	J_{SC} (mA/cm^2)	FF (%)	η (%)
0	0.49	19.73	67.4	6.67
12	0.50	20.37	70.0	7.05
20	0.51	21.37	68.5	7.33
31	0.50	21.62	64.5	6.98

μc-SiO$_x$:H(p) layer. In our case, the cell efficiency of 7.33% was obtained by employing the μc-SiO$_x$:H(p) window layer with [O] of 20 at.% in μc-Si:H single-junction solar cell.

3.3. Application of Different Back Reflecting Layers in μc-Si:H Solar Cells. The back reflector comprising the BRL and metal contact is critical to reflect unabsorbed photons back into the absorber, resulting in the improved long-wavelength absorption and cell performance. The role of BRL was to reduce the parasitic absorption loss of the back reflector. We employed three BRLs in μc-Si:H single-junction solar cells, whose schematic structures are shown in Figure 4.

Figure 5(a) shows the EQE and cell absorptance of μc-Si:H solar cells. Compared to the cell using μc-Si:H(n) as BRL, the cell employing the sputtered ITO as BRL exhibited the lower cell absorptance but slightly higher EQE at wavelengths from 600 to 700 nm. This can be ascribed to the less plasmonic absorption loss by employing ITO than that employing μc-Si:H(n) as BRL [28, 29]. The ITO layer has lower refractive index ($n \sim 2$) than μc-Si:H(n) ($n = 3.1$ at 800 nm), which shifted the plasmonic absorption to short-wavelength region, resulting in the enhanced optical reflection of back reflector. This led to the increase in J_{SC} from 18.95 to 20.01 mA/cm^2 as shown in Table 2. Similar effect was found by using μc-SiO$_x$:H(n) ($n = 2.55$ at 800 nm) as BRL. Compared with the cell employing μc-Si:H(n) as BRL, the cell with μc-SiO$_x$:H(n) exhibited significantly improved EQE from 500 to 1000 nm, which was due to the reduction in plasmonic absorption loss. J_{SC} was significantly increased from 18.95 to 20.83 mA/cm^2. On the other hand, in comparison to the cell employing the ITO layer as BRL, the cell using μc-SiO$_x$:H(n) as BRL ([O] of 27 at.%) exhibited higher absorptance and EQE. This enhancement in EQE was likely due to the improved interface quality by the in situ fabrication process, which avoided the sputtering damage and reduced the formation of native oxide at the interface [11, 30].

In order to have a clear picture on the carrier collection of μc-Si:H solar cells by employing different BRLs, the internal quantum efficiency (IQE) of μc-Si:H solar cells is demonstrated in Figure 5(b). The IQE denoted the ratio of the collected charge carriers to the absorbed photons by the solar cells. Compared to the case using μc-Si:H(n) as BRL, the enhancement of IQE from 600 to 750 nm was due to the reduction in the parasitic absorption loss near the BRL/Ag interface, which led to the more photons being reflected back to the absorber.

Similar to the case using ITO layer, the cell with μc-SiO$_x$:H(n) as BRL exhibited significantly enhanced IQE

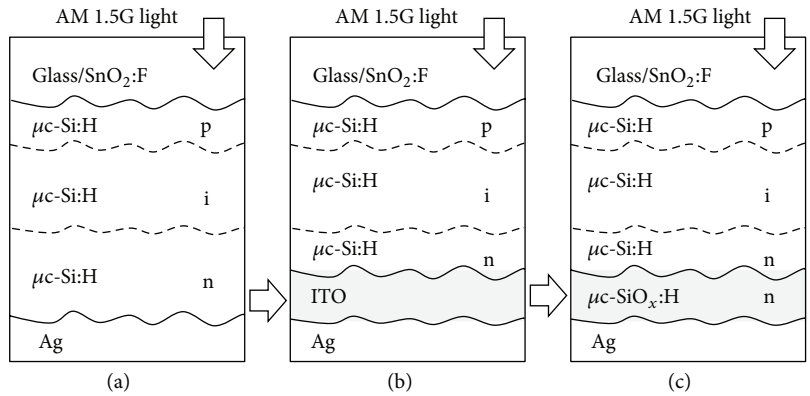

FIGURE 4: Structures of μc-Si:H single-junction solar cells with different BRLs showing (a) the reference cell with μc-Si:H(n) as n-layer and BRL, (b) the cell employing ITO as BRL, and (c) the cell using μc-SiO$_x$:H(n) as a replacement for ITO as BRL.

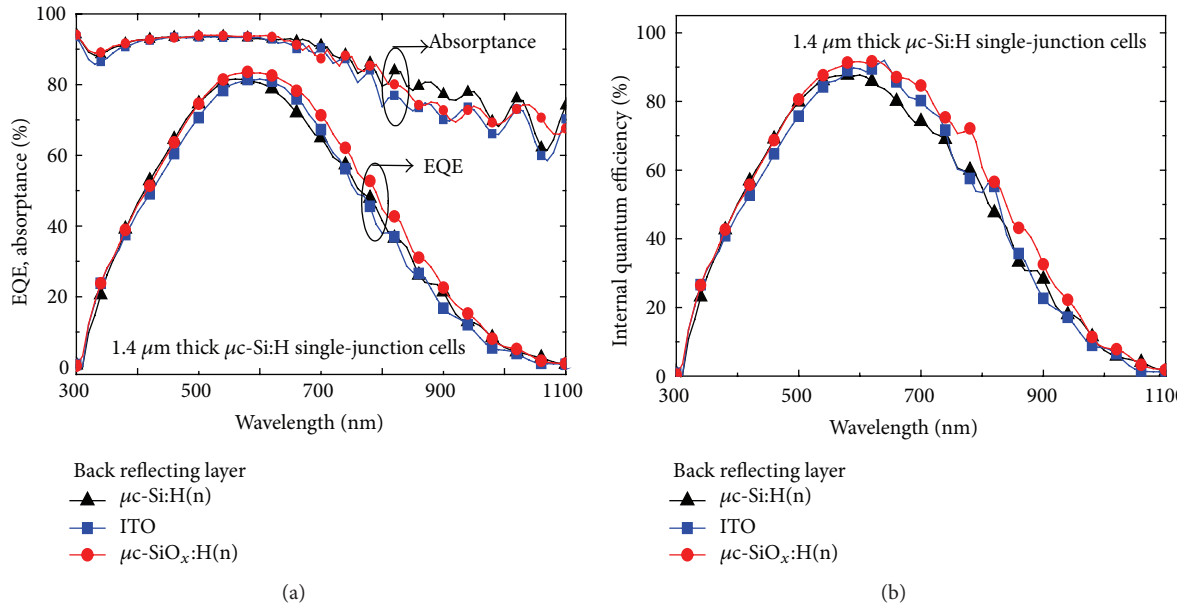

FIGURE 5: (a) External quantum efficiency and absorptance. (b) Internal quantum efficiency of μc-Si:H single-junction solar cells with different BRLs.

TABLE 2: Performance of μc-Si:H single-junction solar cells with different BRLs.

BRL	V_{OC} (V)	J_{SC} (mA/cm^2)	FF (%)	η (%)
μc-Si:H(n)	0.48	18.95	68.2	6.27
ITO	0.48	20.01	68.2	6.55
μc-SiO$_x$:H(n)	0.50	20.83	70.0	7.20

compared with the cell using μc-Si:H(n). This was due to the reduction in parasitic absorption loss by shifting the plasmonic absorption to the less-critical spectral range. In addition, by replacing ITO with μc-SiO$_x$:H(n) as BRL, the IQE was enhanced at the wavelength ranging from 450 to 1100 nm. This manifested that the carrier collection was improved owing to the removal of sputtering damage and the contamination during the air exposure. In our case, the optimized cell efficiency of 7.2% with V_{OC} of 0.5 V, J_{SC} of 20.83 mA/cm^2 and FF of 70.0% was obtained by employing the μc-SiO$_x$:H(n) as BRL in μc-Si:H single-junction solar cell.

3.4. Optimization of a-Si:H/μc-Si:H Solar Cells by Employing Different p-Layer and Back Reflecting Layer in Bottom Cell. The schematic structures of a-Si:H/μc-Si:H tandem cells with different p-layers and BRLs in μc-Si:H bottom cells are shown in Figure 6. The EQE of a-Si:H/μc-Si:H tandem cell employing different p-layers and BRLs in the bottom cell are illustrated in Figure 7. As can be seen, compared to the tandem cell using μc-Si:H(n) as BRL, the cell employing the sputtered ITO as BRL exhibited higher spectral response in wavelengths ranging from 600 to 1000 nm. This was coincided with the results shown in Figure 5, which was due to the decreased plasmonic absorption loss by employing the ITO layer. Therefore, J_{SC} of bottom cell was increased from 9.78 to 10.62 mA/cm^2 as shown in Table 3. The employment

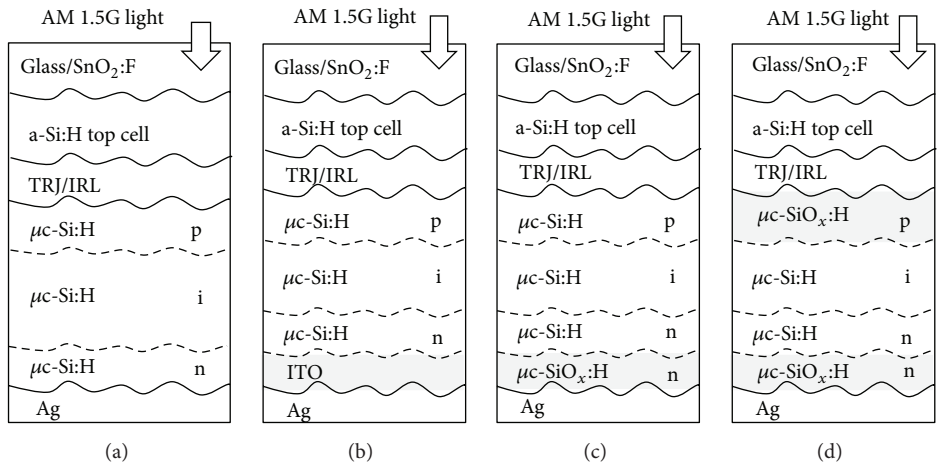

Figure 6: Structures of a-Si:H/μc-Si:H tandem solar cells with different p-layers of bottom cell and BRLs showing (a) the reference cell with μc-Si:H(p) and μc-Si:H(n) in bottom cell, (b) the cell employing ITO as BRL, (c) the cell using μc-SiO_x:H(n) as a replacement for ITO as BRL, and (d) the cell using μc-SiO_x:H(p) as a replacement for μc-Si:H(p).

Table 3: Comparison of the cell performances of a-Si:H/μc-Si:H tandem cell with different p-layers of bottom cell and BRLs.

p-layer (bottom cell)	BRL	V_{OC} (V)	J_{SC} (mA/cm^2)	$J_{QE,top}$ (mA/cm^2)	$J_{QE,bot.}$ (mA/cm^2)	$J_{QE,total}$ (mA/cm^2)	FF (%)	η (%)
μc-Si:H(p)	μc-Si:H(n)	1.34	9.70	11.47	9.78	21.25	69.9	9.06
μc-Si:H(p)	ITO	1.35	10.11	11.45	10.62	22.07	71.1	9.94
μc-Si:H(p)	μc-SiO_x:H(n)	1.35	10.62	11.52	11.58	23.10	71.9	10.27
μc-SiO_x:H(p)	μc-SiO_x:H(n)	1.37	10.55	11.57	13.08	24.65	73.7	10.51

of μc-SiO_x:H(n) ([O] of 27 at.%) as BRL exhibited similar effect as the case of ITO. Compared to μc-Si:H(n) as BRL, the tandem cell employing μc-SiO_x:H(n) as BRL had a significant enhancement in the spectral response of long-wavelength range, which led to the increase in J_{SC} of bottom cell from 9.78 to 11.58 mA/cm^2. In addition, compared to the sputtered ITO as BRL, the replacement of μc-SiO_x:H(n) as BRL showed higher spectral response from 600 to 1000 nm. The increase of J_{SC} in the bottom cell from 10.62 to 11.58 mA/cm^2 was more likely because of the decreased plasmonic losses by the μc-SiO_x:H(n) as BRL. Another factor could ascribe to the all in situ PECVD process which reduced the interface defects [31].

In addition, the cell with μc-SiO_x:H(p) as the replacement of μc-Si:H(p) of the bottom cell is shown for comparison. The significant enhancement in spectral response of long-wavelength range can be ascribed to two factors. First, the absorption coefficient of μc-SiO_x:H(p) is lower than that of μc-Si:H(p), which resulted in the reduced parasitic absorption loss by the p-layer. Second, the replacement of μc-Si:H(p) by μc-SiO_x:H(p) could increase the build-in field due to the higher optical band gap of μc-SiO_x:H(p), resulting in the increased V_{OC} and the enhanced carrier collection in long-wavelength region. These two factors led to the advanced optical absorption in long-wavelength range, contributing in the significantly enhanced J_{SC} of bottom cell from 11.58 to 13.08 mA/cm^2.

The performance of tandem cell with μc-SiO_x:H(p) replacing μc-Si:H(p) of the bottom cell is shown in Table 3. The increased FF from 71.9 to 73.7% can be ascribed to the shunt quenching effect by the μc-SiO_x:H(p) layer, which led to reduced leakage current of the cell [32]. In addition, the carrier recombination in tunneling recombination junction (TRJ) may be enhanced by replacing μc-Si:H(p) with μc-SiO_x:H(p), resulting in the increase in V_{OC} and FF [33]. Combining the effects discussed above, the a-Si:H/μc-Si:H tandem solar cell employing the μc-SiO_x:H(p) as p-layer of bottom cell and μc-SiO_x:H(n) as BRL with efficiency of 10.51%, V_{OC} of 1.37 V, J_{SC} of 10.55 mA/cm^2, and FF of 73.67% was obtained.

4. Conclusion

The p-type and the n-type μc-SiO_x:H with varied [O] have been prepared and employed as window layer and back reflecting layer, respectively, in μc-Si:H single-junction solar cells. Regarding the μc-SiO_x:H films, the decreased refractive index accompanied with the wider E_{04} with increasing [O] can be ascribed to the increased Si-O bond in amorphous silicon oxide phase, while structural defects could disrupt crystalline structure, resulting in the degraded X_C and σ_d.

By utilizing μc-SiO_x:H(p) with increasing [O] in μc-Si:H single-junction solar cell, the short-wavelength spectral response enhanced. However, too much oxygen incorporation induced defects in μc-SiO_x:H(p) which could decrease the V_{OC} and FF. Meanwhile, ITO in μc-Si:H single-junction cell was replaced by the highly conductive μc-SiO_x:H(n) with [O] of 27 at.%. The employment of μc-SiO_x:H(n) enhanced spectral response and increased FF, which were due to the

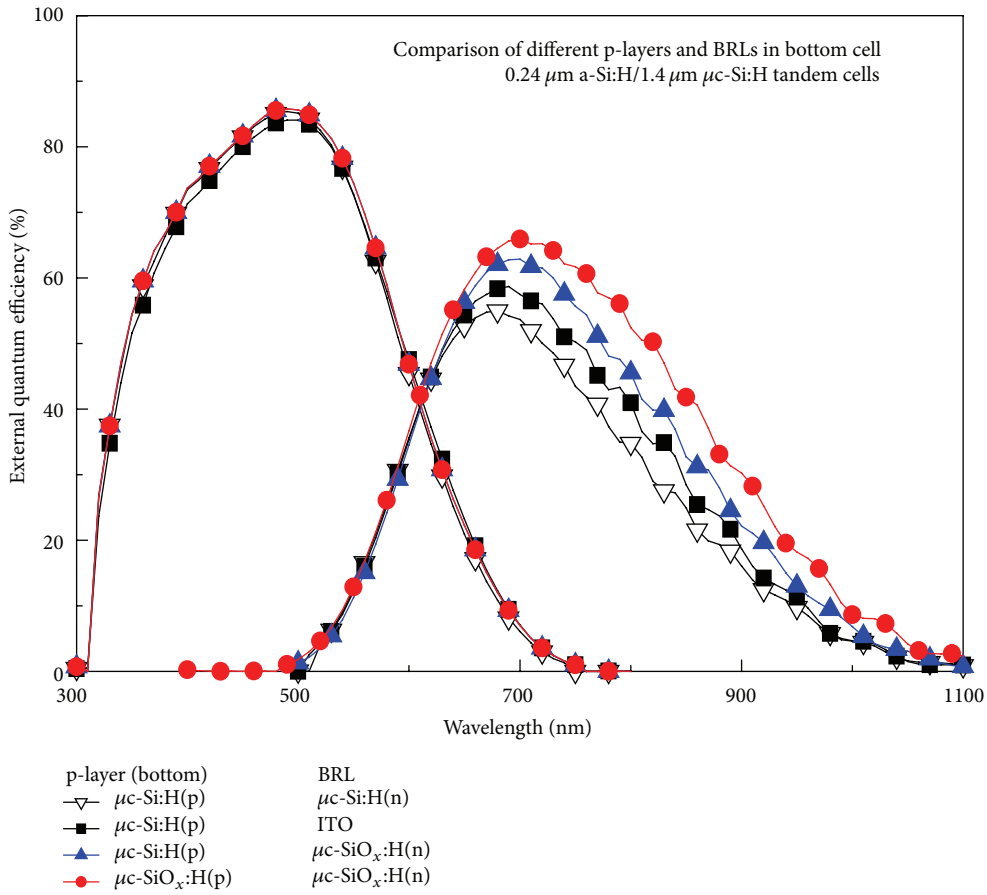

FIGURE 7: External quantum efficiency of a-Si:H/μc-Si:H tandem solar cells employing different p-layers of bottom cell and BRLs.

elimination of ex-situ ITO sputtering step and the unavoidable sputtering damage at the μc-Si:H(n)/ITO interface. Finally, further replacing μc-Si:H(p) by μc-SiO$_x$:H(p) as p-layer of bottom cell enhanced FF and V_{OC}, which might result from the increased carrier recombination between TRJ layers. In addition, the higher J_{SC} of bottom cell can be ascribed to the less parasitic absorption loss of μc-SiO$_x$:H(p) than that of μc-Si:H(p). Compared to the reference cell, the optimized cell efficiency by employing μc-SiO$_x$:H(p) and μc-SiO$_x$:H(n) achieved cell efficiency from 9.06 to 10.51%, with V_{OC} of 1.37 V, J_{SC} of 10.55 mA/cm^2, and FF of 73.67%, which had a relative efficiency enhancement of 16%.

Competing Interests

The authors do not have any competing interests concerning the content of the paper.

Acknowledgments

This work was sponsored by Ministry of Science and Technology in Taiwan under Grant no. 103-3113-P-008-001. Besides, the authors gratefully thank Hung-Jung Hsu for continuous support and encouragement.

References

[1] K. L. Chopra, P. D. Paulson, and V. Dutta, "Thin-film solar cells: an overview," *Progress in Photovoltaics: Research and Applications*, vol. 12, no. 2-3, pp. 69–92, 2004.

[2] A. V. Shah, H. Schade, M. Vanecek et al., "Thin-film silicon solar cell technology," *Progress in Photovoltaics: Research and Applications*, vol. 12, no. 2-3, pp. 113–142, 2004.

[3] A. V. Shah, J. Meier, E. Vallat-Sauvain et al., "Material and solar cell research in microcrystalline silicon," *Solar Energy Materials & Solar Cells*, vol. 78, no. 1–4, pp. 469–491, 2003.

[4] H. Keppner, J. Meier, P. Torres, D. Fischer, and A. Shah, "Microcrystalline silicon and micromorph tandem solar cells," *Applied Physics A: Materials Science and Processing*, vol. 69, no. 2, pp. 169–177, 1999.

[5] K. Yamamoto, A. Nakajima, M. Yoshimi et al., "A thin-film silicon solar cell and module," *Progress in Photovoltaics: Research and Application*, vol. 13, no. 6, pp. 489–494, 2005.

[6] K. Ding, T. Kirchartz, B. E. Pieters et al., "Characterization and simulation of a-Si:H/μc-Si:H tandem solar cells," *Solar Energy Materials and Solar Cells*, vol. 95, no. 12, pp. 3318–3327, 2011.

[7] R. E. Hollingsworth and P. K. Bhat, "Doped microcrystalline silicon growth by high frequency plasmas," *Applied Physics Letters*, vol. 64, no. 5, pp. 616–618, 1994.

[8] S. C. Saha and S. Ray, "Development of highly conductive n–type μc–Si:H films at low power for device applications," *Journal of Applied Physics*, vol. 78, no. 9, pp. 5713–5720, 1995.

[9] J. K. Rath and R. E. I. Schropp, "Incorporation of p-type microcrystalline silicon films in amorphous silicon based solar cells in a superstrate structure," *Solar Energy Materials and Solar Cells*, vol. 53, no. 1-2, pp. 189–203, 1998.

[10] S. C. Saha, A. K. Barua, and S. Ray, "The role of hydrogen dilution and radio frequency power in the formation of microcrystallinity of n-type Si:H thin film," *Journal of Applied Physics*, vol. 74, no. 9, pp. 5561–5568, 1993.

[11] G. Lucovsky, J. Yang, S. S. Chao, J. E. Tyler, and W. Czubatyj, "Oxygen-bonding environments in glow-discharge-deposited amorphous silicon-hydrogen alloy films," *Physical Review B*, vol. 28, no. 6, pp. 3225–3233, 1983.

[12] P. Cuony, M. Marending, D. T. L. Alexander et al., "Mixed-phase p-type silicon oxide containing silicon nanocrystals and its role in thin-film silicon solar cells," *Applied Physics Letters*, vol. 97, no. 21, Article ID 213502, 2010.

[13] L. V. Mercaldo, P. Delli Veneri, I. Usatii, E. M. Esposito, and G. Nicotra, "Properties of mixed phase n-doped silicon oxide layers and application in micromorph solar cells," *Solar Energy Materials and Solar Cells*, vol. 119, pp. 67–72, 2013.

[14] A. Sarker, C. Banerjee, and A. K. Barua, "Preparation and characterization of n-type microcrystalline hydrogenated silicon oxide films," *Journal of Physics D: Applied Physics*, vol. 35, no. 11, pp. 1205–1209, 2002.

[15] V. Smirnov, W. Böttler, A. Lambertz, H. Wang, R. Carius, and F. Finger, "Microcrystalline silicon n-i-p solar cells prepared with microcrystalline silicon oxide (μc-SiOx:H) n-layer," *Physica Status Solidi (C) Current Topics in Solid State Physics*, vol. 7, no. 3-4, pp. 1053–1056, 2010.

[16] T. Krajangsang, S. Kasashima, A. Hongsingthong, P. Sichanugrist, and M. Konagai, "Effect of p-μc-$Si_{1-x}O_x$:H layer on performance of hetero-junction microcrystalline silicon solar cells under light concentration," *Current Applied Physics*, vol. 12, pp. 515–520, 2012.

[17] A. Lambertz, T. Grundler, and F. Finger, "Hydrogenated amorphous silicon oxide containing a microcrystalline silicon phase and usage as an intermediate reflector in thin-film silicon solar cells," *Journal of Applied Physics*, vol. 109, no. 11, Article ID 113109, 2011.

[18] C. Zhang, M. Meier, A. Lambertz et al., "Optical and electrical effects of p-type c-SiO_x:H in thin-film silicon solar cells on various front textures," *International Journal of Photoenergy*, vol. 2014, Article ID 176965, 10 pages, 2014.

[19] V. Smirnov, A. Lambertz, S. Tillmanns, and F. Finger, "p- and n-type microcrystalline silicon oxide (μc-SiO_x:H) for application in thin film silicon tandem solar cells," *Canadian Journal of Physics*, vol. 92, pp. 932–935, 2014.

[20] S. W. Liang, *Development and optimization of microcrystalline silicon thin-film solar cells with microcrystalline silicon oxide as N-type and back reflecting layer and its application in multi-junction devices [Ph.D. thesis]*, Department of Photonics and Institute of Electro-Optical Engineering, National Chiao Tung University, 2014.

[21] D. Das, M. Jana, and A. K. Barua, "Characterization of undoped μc-SiO:H films prepared from (SiH_4+CO_2+H_2)-plasma in RF glow discharge," *Solar Energy Materials & Solar Cells*, vol. 63, no. 3, pp. 285–297, 2000.

[22] F. Demichelis, C. F. Pirri, and E. Tresso, "Influence of doping on the structural and optoelectronic properties of amorphous and microcrystalline silicon carbide," *Journal of Applied Physics*, vol. 72, no. 4, pp. 1327–1333, 1992.

[23] D. Adler, "Density of states in the gap of tetrahedrally bonded amorphous semiconductors," *Physical Review Letters*, vol. 41, no. 25, pp. 1755–1758, 1978.

[24] T. Hamasaki, M. Ueda, Y. Osaka, and M. Hirose, "Preferential segregation of dopants in μc-Si:H," *Journal of Non-Crystalline Solids*, vol. 59-60, no. 2, pp. 811–814, 1983.

[25] L. Xiao, O. Astakhov, R. Carius, A. Lambertz, T. Grundler, and F. Finger, "Defects and structure of μc-SiO_x:H deposited by PECVD," *Physica Status Solidi C*, vol. 7, no. 3-4, pp. 941–944, 2010.

[26] K. Schwanitz, S. Klein, T. Stolley, M. Rohde, D. Severin, and R. Trassl, "Anti-reflective microcrystalline silicon oxide p-layer for thin-film silicon solar cells on ZnO," *Solar Energy Materials and Solar Cells*, vol. 105, pp. 187–191, 2012.

[27] R. Biron, C. Pahud, F.-J. Haug, J. Escarré, K. Söderström, and C. Ballif, "Window layer with p doped silicon oxide for high V_{OC} thin-film silicon n-i-p solar cells," *Journal of Applied Physics*, vol. 110, no. 12, Article ID 124511, 2011.

[28] U. Palanchoke, V. Jovanov, H. Kurz, P. Obermeyer, H. Stiebig, and D. Knipp, "Plasmonic effects in amorphous silicon thin film solar cells with metal back contacts," *Optics Express*, vol. 20, no. 6, pp. 6340–6347, 2012.

[29] F.-J. Haug, T. Söderström, O. Cubero, V. Terrazzoni-Daudrix, and C. Ballif, "Plasmonic absorption in textured silver back reflectors of thin film solar cells," *Journal of Applied Physics*, vol. 104, no. 6, Article ID 064509, 2008.

[30] T. Söderström, F.-J. Haug, X. Niquille, and C. Ballif, "TCOs for Nip thin film silicon solar cells," *Progress in Photovoltaics: Research and Applications*, vol. 17, no. 3, pp. 165–176, 2009.

[31] B. Demaurex, S. De Wolf, A. Descoeudres, Z. C. Holman, and C. Ballif, "Damage at hydrogenated amorphous/crystalline silicon interfaces by indium tin oxide overlayer sputtering," *Applied Physics Letters*, vol. 101, no. 17, Article ID 171604, 2012.

[32] M. Despeisse, C. Battaglia, M. Boccard et al., "Optimization of thin film silicon solar cells on highly textured substrates," *Physica Status Solidi A*, vol. 208, no. 8, pp. 1863–1868, 2011.

[33] B. Bills, X. Liao, D. W. Galipeau, and Q. H. Fan, "Effect of tunnel recombination junction on crossover between the dark and illuminated current-voltage curves of tandem solar cells," *IEEE Transactions on Electron Devices*, vol. 59, no. 9, pp. 2327–2330, 2012.